Soft Matter

Accepted Manuscript

ROYAL SOCIETY OF CHEMISTRY

www.rsc.org/softmatter

Graphical Abstract

Synthesis, nanoprecipitation and pH sensitivity of amphiphilic linear-dendritic hybrid polymers and hyperbranched-polydendrons containing tertiary amine functional dendrons

Hannah E. Rogers, Pierre Chambon, Sam E. R. Auty, Faye Y. Hern, Andrew Owen and Steve P. Rannard[a*]

Tertiary amine functional dendron initiators have been used to create hyperbranched-polydendrons with an pH-responsive chain end and hydrophobic core. The materials self-assemble under nanoprecipitation conditions to form nanoparticles with behaviour that varies from analogous particles made using linear-dendritic hybrids

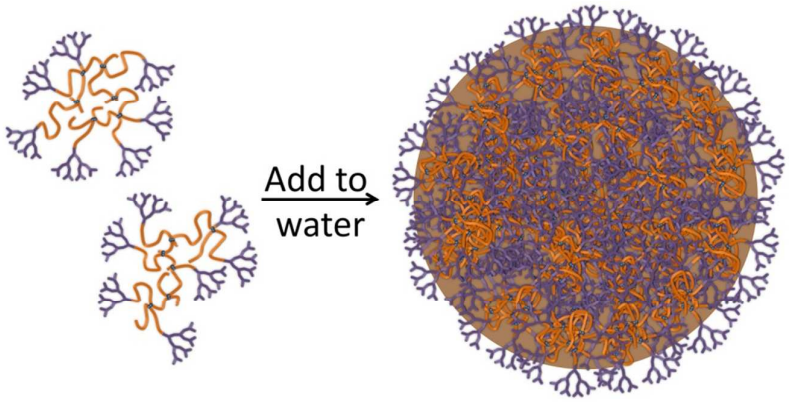

Journal Name

RSCPublishing

ARTICLE

Synthesis, nanoprecipitation and pH sensitivity of amphiphilic linear-dendritic hybrid polymers and hyperbranched-polydendrons containing tertiary amine functional dendrons

Cite this: DOI: 10.1039/xoxxoooooox

Received ooth January 2012,
Accepted ooth January 2012

DOI: 10.1039/xoxxoooooox

www.rsc.org/

Hannah E. Rogers,[a] Pierre Chambon,[a] Sam E. R. Auty,[a] Faye Y. Hern,[a] Andrew Owen[b] and Steve P. Rannard[a]*

The combination of linear polymers with dendritic chain-ends has led to numerous studies of linear-dendritic polymer hybrid materials. Interchain branching within the linear segment of these materials has recently extended this concept to the formation of soluble hyperbranched-polydendrons. Here, the introduction of amphiphilicity into hyperbranched-polydendrons has been achieved for the first time through the use of tertiary amine functional dendritic chain-ends and branched hydrophobic polymer segments. The synthesis and aqueous nanoprecipitation of these branched materials is compared with their linear-dendritic polymer analogues, showing that chain-end chemistry/generation, precipitation medium pH and polymer architecture are all capable of influencing the ability to generate nanoparticles, the resulting nanoparticle diameter and dispersity, and subsequent response to changes in pH.

Introduction

The introduction of synthetic approaches to ideally branched dendrimers and non-uniform hyperbranched polymers generated a new global theme for macromolecular architectural study over three decades ago.[1-3] Although the near-perfect branching within dendrimers is highly appealing for applications from sensor coatings to solar energy conversion and nanomedicine,[4-6] the convergent and divergent synthesis routes are both hampered by considerable synthetic challenges including structural imperfections at high generations, multiple, iterative experimental steps and the use of large excesses of reagents.[7-9] Convergent growth allows very high levels of control over internal chemistry and surface functionality but, especially at high generations, conventional synthesis routes enable successive doubling of molecular weight but very little increase in sample mass after each step.[10-13] In contrast, divergent growth leads to large increases in both the molecular weight of the material and its physical sample mass but an exponentially increasing number of reactions are required at the periphery of growing macromolecule, leading to difficulty in accurate attainment of each generation;[14,15a] recent application of "click" chemistries have been shown to present options to overcome many of these synthetic issues.[15b]

Dendrons, the major structural components of dendrimers, have been combined with linear polymers to generate various new classes of complex polymer architectures. These include the introduction of dendrons as pendant side chains,[16,17] to produce dendronised polymers, and the placement of dendrons at linear polymer chain-ends,[18-20] to form linear-dendritic polymer hybrids. Very recently we reported the introduction of simultaneous branching during the propagation of the vinyl segment of a linear-dendritic hybrid, to form a new class of macromolecular architecture; hyperbranched-polydendrons (*hyp*-polydendrons).[21-22] Inspired by the extension of the conventional free-radical "Strathclyde" polymerisation approach to branched-vinyl polymers,[23,24] the use of a dendron macroinitiator within the controlled radical copolymerisation of a mixture of vinyl and divinyl monomers has been used to form soluble, high molecular weight ($M_w > 10^6$ g/mol) branched vinyl polymers bearing an ideally synthesised dendron at one end of every conjoined chain. This approach to branched vinyl polymers differs from self-condensing vinyl polymerisation[25,26] in several ways, not least that each primary polymer chain has two free chain-ends.

The combination of chain or step growth polymers with dendron precursors allows the attainment of significant sample masses, high functionality and high molecular weights within a relatively small number of synthetic steps. A compromise in the ideal nature of the branching throughout the macromolecule is required; however, *hyp*-polydendrons have been shown to generate new material options and behave concertedly to generate uniform nanoparticles despite complexity within their chemistry and molecular weight distribution.[21,22]

Herein we present the first comparative study of linear-dendritic hybrid polymers and their *hyp*-polydendron analogues comprising tertiary amine-functional dendron chain-ends and hydrophobic vinyl polymer segments. Three new low generation dendron initiators have been synthesised and copper-catalysed, methanolic atom transfer radical polymerisation (ATRP) has been employed in either the polymerisation of 2-hydroxypropyl methacrylate (HPMA) or the copolymerisation of HPMA with ethylene glycol dimethacrylate (EGDMA). Nanoprecipitation approaches have been applied to form aqueous dispersions of nanoparticles from each material synthesised and the influence of polymer architecture and solution pH have been studied.

Results and Discussion

Synthesis of 1-[N, N-bis(2-aminopropyl)-amino]-2-propanol (6).

The strategy devised for the synthesis of tertiary amine-functional dendritic ATRP initiators required the Michael addition of 2-(dimethylamino) ethyl acrylate (DMEA) to primary amine-containing dendrons also bearing secondary hydroxyl functionality. In previous reports, we synthesised an AB_2 monomer comprising such a mixture of primary amines and secondary hydroxyls,[27,28] using diethylene triamine and propylene glycol, and opted to use this strategy again with slight modification (Scheme 1).

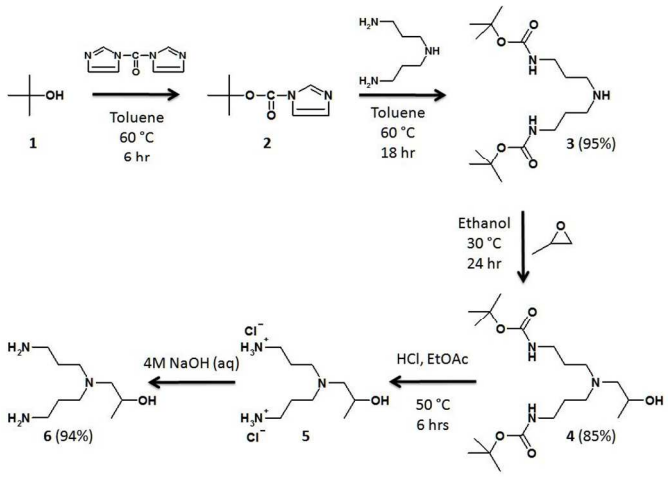

Scheme 1. Selective synthesis of a new AB_2 branching molecule, **6**, bearing primary amine and secondary hydroxyl functionality

Briefly, *t*-butanol **1** was reacted with 1,1'-carbonyl diimidazole to form the subsequent imidazole carboxylic ester mono-adduct **2**, avoiding coupling of **1** to form the symmetrical carbonate, and in high yield as previously described.[29] Selective reaction of **2** with the primary amine groups within dipropylenetriamine allowed the formation of the *t*-butyloxycarbonyl (*t*-BOC) protected product **3**, avoiding reaction at the secondary amine functionality. The addition of propylene oxide in ethanol to **3** resulted in the introduction of a secondary hydroxyl group **4**, and subsequent removal of the *t*-BOC groups led to the desired AB_2 product **6**, via the hydrochloride salt **5**. The reactions were monitored by thin layer chromatography, ^{1}H and ^{13}C nuclear magnetic resonance spectroscopy (NMR), 2D ^{1}H-^{1}H Correlated Spectroscopy (COSY) NMR and electrospray or chemical-ionisation mass spectrometry (ES-MS/CI-MS; Electronic Supplementary Information (ESI) Figs S1-10).

Synthesis of tertiary amine functional dendron ATRP initiators (11, 12 and 13).

As mentioned previously, our synthesis strategy aimed to employ the simple Michael addition of DMEA to primary amines and a series of target tertiary amine functional initiators was designed, ranging from the zeroth to the second generation (G_0-G_2), which had significant chemical similarity and utilised either 1-dimethylamino-2-propanol **7**, 1-amino-2-propanol **8** or **6** (Scheme 2).

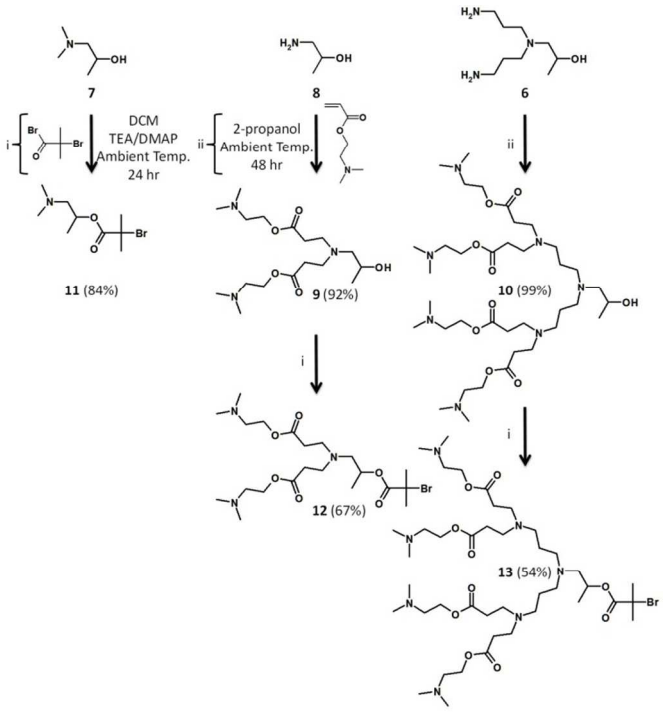

Scheme 2. Synthesis of three generations of dendritic atom transfer radical polymerisation initiators (**11**-**13**) bearing tertiary amine surface functionality.

The simple reaction of α-bromoisobutyryl bromide (BiB) with **7** led to the G_0-Br initiator **11** without complication (ESI Figs S11-13) as confirmed by ^{1}H and ^{13}C NMR and electrospray mass spectrometry (MH^+ = 252.1 Da). The G_1-Br dendron initiator **12** required two steps, including the initial exhaustive Michael addition of DMEA with **8** which proceeded smoothly using a 6-fold molar excess of DMEA and requiring just the removal of solvent and unreacted DMEA under vacuum to give the tertiary amine functional dendron G_1-OH **9** (ESI Figs S14-16; ES-MS: MH^+ = 362.3 Da, MNa^+ = 384.3 Da). ^{1}H NMR confirmed the lack of vinyl resonances ($\delta \sim 6$ ppm), corresponding to DMEA impurities, the appearance of a strong singlet peak ($\delta = 2.26$ ppm) assigned to the four amino methyl groups of the added acrylate, and the upfield shift of the doublet of doublets resonance corresponding to the methylene protons

neighbouring the primary amine group of **8**. Reaction of **9** with BiB, under identical conditions to those used to form **11**, generated the target dendron initiator **12** with 67% recovered yield (ESI Figs S17-19; ES-MS: MH+ = 510.2 Da, MNa^+ = 534.2 Da). The ^{1}H NMR resonance of the methine proton adjacent to the secondary hydroxyl group was observed to move from δ = 3.87 ppm to δ = 5.04 ppm upon esterification and the two methyl groups of the α-bromoester were observed at δ = 1.89 ppm. This identical strategy was used to react **6** with DMEA; a 3-fold molar excess per primary amine was required to allow the exhaustive Michael addition to yield the G_2-OH dendron **10** (ESI Figs S20-22; ES-MS: MH^+ = 762.6 Da, MNa^+ = 784.6 Da). Again, esterification of the hydroxyl focal point of **10** led to the G_2-Br initiator **13** in 54% recovered yield (ESI Figs S23-25,Table S1; ES-MS: MH^+ = 912.5 Da, MNa^+ = 934.5 Da, MK^+ = 950.5 Da). This straightforward approach to low generation dendron initiator synthesis proved robust and highly reproducible and has been repeatedly conducted on a multi-gram scale.

Linear polymerisation and branched copolymerisation of HPMA and EGDMA using ethyl and G_0-G_2 tertiary amine functional dendron ATRP initiators.

In previous studies, a number average degree of polymerisation (DP_n) of 50 monomer units has been shown to yield linear-dendritic polymers and *hyp*-polydendrons from HPMA that undergo nanoprecipitation into water,[30] therefore, this chain length was targeted for all polymers within this study to allow comparison with previous reports (Figure 1). Copper/bypridyl (bpy) catalysed ATRP, conducted at 30 °C in methanol at a concentration of 35% w/v relative to monomer, was also chosen due to previous successful polymerisation of this monomer under these conditions ([initiator]:[HPMA]:[Cu(I)Cl]:[bpy]= 1:50:1:2).[21,22,30] To allow for comparison with unfunctionalised materials, the commercially available initiator ethyl α-bromoisobutyrate (EBiB) was also used to initiate the linear polymerisation, and branched copolymerisation, of HPMA.

The formation of the linear polymer and linear-dendritic hybrids using EBiB and the dendron initiators **11**, **12** and **13**, (Figure 1A) generated polymers at high monomer conversion (>94 %) as determined by ^{1}H NMR of the crude polymerisations. As is often common with ATRP, the recovered polymers showed higher number average molecular weights (M_n) than targeted (Table 1), but monomodal distributions were observed in all refractive index chromatograms during triple detection size exclusion chromatography (SEC) analyses and values were consistent with earlier reports (ESI Fig S26).[30] Despite these high M_n values, which may indicate relatively poor initiator efficiencies, the linear polymer series were consistent in their achieved DP_n allowing an accurate assessment of material behaviour with respect to differences in chain-end functionality. Kinetic studies indicated first order kinetics for all linear polymerisations and linear evolution of M_n with conversion (ESI Fig S27). Interestingly, the polymerisations initiated by G_1-Br (**12**) and G_2-Br (**13**) appeared to propagate faster than reactions using the other initiators, achieving approximately 90% conversion in 5 hours; the EBiB and G_0-Br polymerisations showed very similar kinetics. Dispersity (Đ) values were relatively consistent from 40% monomer conversion, although values tended to be 1.45 > Đ > 1.2.

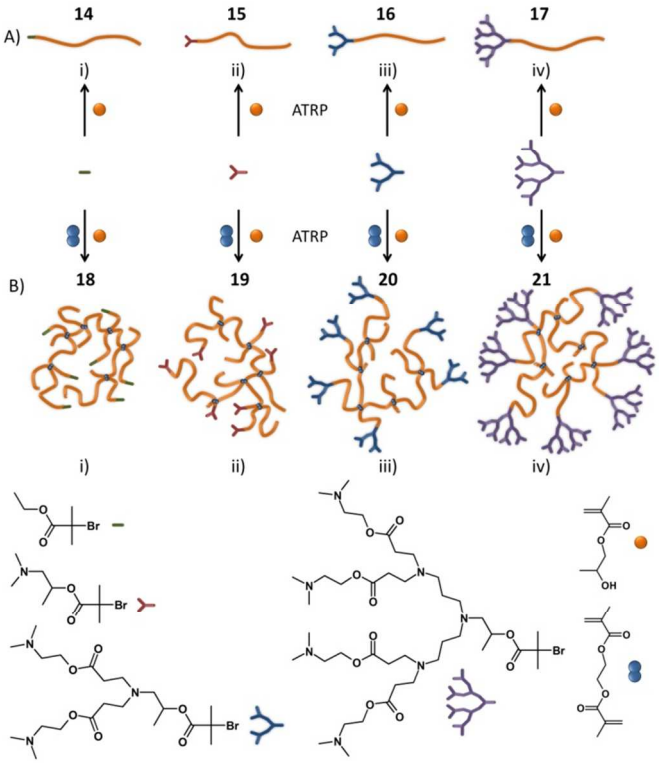

Figure 1. Diagrammatic representation of the use of ethyl α-bromoisobutyrate and three generations of amine functional dendron initiators for; A) the polymerisation of HPMA to form linear polymers and linear-dendritic hybrid polymers (**14**-**17**), and B) copolymerisation of HPMA and EGDMA to form branched polymers and hyperbranched polydendrons (**18**-**21**).

The branched copolymerisation of HPMA and EGDMA was conducted under identical conditions to those used for linear-dendritic polymer synthesis, but with the addition of a low concentration of EGDMA (Figure 1B). When using EBiB as the initiator, a molar ratio of brancher:initiator of 0.95:1 was employed and high molecular weight, soluble polymer (**18**) was recovered (Table 1). When using the G_0-Br, G_1-Br and G_2-Br initiators **11**-**13**, gel formation was seen within the HPMA/EGDMA copolymerisations at this ratio but soluble *hyp*-polydendrons (**19**, **20**, **21**) were achieved at lower brancher:initiator ratios (0.90:1) again suggesting a lower initiator efficiency, as poor initiation will lead to fewer propagating polymer chains and a higher effective brancher:chain ratio within each reaction.

Kinetic studies of the branched copolymerisations initiated by either EBiB or G_0-Br showed almost identical polymerisation rates as the respective linear polymerisations conducted in the absence of EGDMA (ESI Fig S28); however, *hyp*-polydendron synthesis using the G_1-Br and G_2-Br initiators propagated noticeably slower than their analogous linear-dendritic polymer reactions. Molecular weight analyses were

enabled by determining average dn/dc values (ESI Table S2). Linear semilog plots were observed within the branched polymerisations using each of the initiators, confirming first order kinetics (ESI Fig S28); the development of M_n and weight average molecular weight (M_w) within the branched polymerisations showed the well reported[30,31] dramatic increase at conversions >80 % which was very noticeable within the relationship of M_w and conversion and leading to multimodal SEC chromatograms (ESI Fig S29). M_w values up to 1.02×10^6 g/mol were observed, suggesting significant contributions to the physical mass of each sample from complex branched structures containing on average > 80 primary chains (**18**), > 65 primary chains (**19**), > 45 primary chains (**20**) and > 17 primary chains (**21**). Number average structures appear to contain at least 3 conjoined chains. Each primary chain of the *hyp*-polydendrons **19**, **20** and **21** contains a dendron initiator end group, therefore the weight average branched architectures contain approximately 65 tertiary amines (**19**), 90 tertiary amines (**20**) or 68 tertiary amine (**21**) chain-end functional groups.

Table 1. SEC analysis of amine-functional linear-dendritic hybrids (**15-17**) and *hyp*-polydendrons (**19-21**) and materials without amine end group functionality (**14** and **18**).

Target polymer	M_n Theory (g/mol)	SEC[a] M_n (g/mol)	SEC[a] M_w (g/mol)	SEC[a] Đ	SEC[a] DP_n
EBiB-*p*(HPMA$_{50}$), **14**	7100	12770	15840	1.24	87
G$_0$-*p*(HPMA$_{50}$), **15**	7390	11250	16320	1.45	76
G$_1$-*p*(HPMA$_{50}$), **16**	7430	13170	18070	1.37	88
G$_2$-*p*(HPMA$_{50}$), **17**	7690	12910	16330	1.26	83
EBiB-*p*(HPMA$_{50}$-*co*-EGDMA$_{0.95}$), **18**	-	39760	1019000	22.63	-
G$_0$-*p*(HPMA$_{50}$-*co*-EGDMA$_{0.9}$), **19**	-	33580	728540	21.70	-
G$_1$-*p*(HPMA$_{50}$-*co*-EGDMA$_{0.9}$), **20**	-	46820	595190	12.71	-
G$_2$-*p*(HPMA$_{50}$-*co*-EGDMA$_{0.9}$), **21**	-	37530	216400	5.77	-

[a]THF eluent containing 2% TEA (v/v)

Comparative nanoprecipitation studies of linear polymers, linear-dendritic hybrids, branched copolymers and hyperbranched-polydendrons.

The assembly of linear-dendritic polymers, including stimuli-responsive materials, has received increasing attention and has been the subject of a range of detailed reviews.[32,33] Examples of water-soluble linear polymer segments with hydrophobic dendritic chain-ends have been shown to form micelles[34] and "worm-like" structures[35] driven by the hydrophobicity of the dendrons and thermally responsive behaviour of the linear polymer chains. More complex structures containing hydrophobic dendrons decorated with hydrophilic poly(ethylene glycol) (PEG) chains, and bearing a single hydrophilic but thermo-responsive linear poly(2-(2'-methoxyethoxy) ethyl methacrylate) chain, have also been reported as forming micelles upon heating; stabilised by the peripheral PEG groups.[36] pH-Responsive self-assembled structures have been described including materials that bear primary amines on the dendritic segment and single hydrophobic linear chains,[37] tertiary amines within the dendron core structure decorated with PEG peripheral groups and polycaprolactone hydrophobic linear chains,[38] and structures bearing oppositely charged peptide chains at the periphery and focal point of amido-amine functional dendrons.[39] Other routes to pH-responsive behaviour includes introducing the response during the cleavage of protecting groups from the surface of dendrons[40] or hyperbranched polymer components.[41]

In many cases, the formation of self-assembled structures is accomplished by dissolution within a water-miscible solvent such as dimethylformamide[42] or tetrahydrofuran[34] with subsequent slow dialysis to remove the good solvent for both components of the linear-dendritic polymer hybrid. As mentioned previously, we have recently investigated nanoprecipitation[21,22,30] as a rapid and straightforward approach to the formation of branched polymer nanoparticles and have extended this research to include the materials within this study. Aqueous nanoprecipitation requires the mixing (slow or rapid) of a polymer dissolved in a good, water-miscible solvent with water (acting as anti-solvent).[43] A nucleation and growth mechanism is proposed (Figure 2) whereby the expanded polymer coils collapse, as the liquid media rapidly diffuse together and the quality of the solvent environment decreases.[44,45]

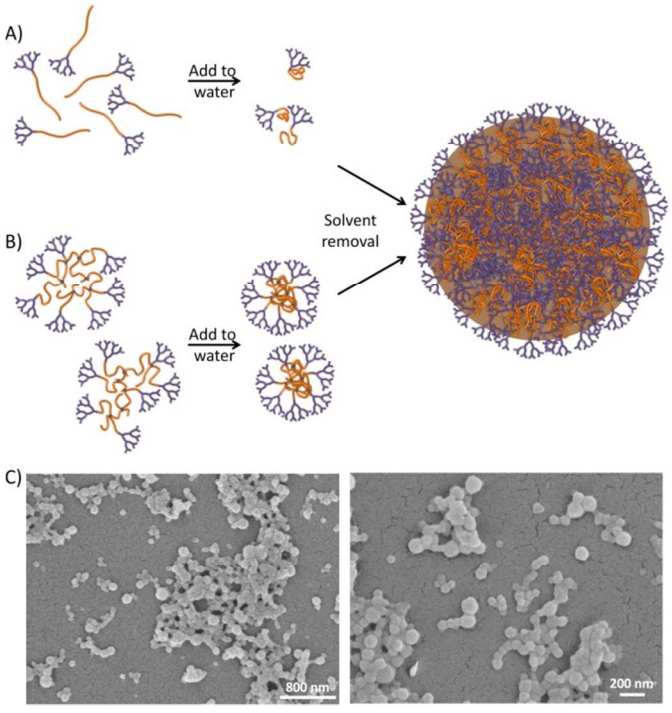

Figure 2. Diagrammatic representation of the nanoprecipitation of A) linear-dendritic hybrids, and B) hyperbranched-polydendrons derived from amine-functional dendron initiators. C) Representative SEM images of nanoprecipitated G$_2$-*p*(HPMA$_{50}$-*co*-EGDMA$_{0.9}$) formed from an initial THF concentration of 5 mg mL^{-1} producing an aqueous concentration of 1 mg mL^{-1} at pH = 7.8.

The nuclei will assemble into larger aggregates, with collapsed unimers also associating with the larger particles as they

grow.[44] Colloidal stability must be achieved, usually through steric or charge repulsion, or macroscale precipitation will occur.[43,44]

Initially, the simple nanoprecipitation of the linear and branched, EBiB-initiated polymers EBiB-*p*(HPMA$_{50}$), **14**, and EBiB-*p*(HPMA$_{50}$-*co*-EGDMA$_{0.95}$), **18**, was conducted by dissolving the polymers individually into tetrahydrofuran (THF) at a concentration of 5 mg mL^{-1} and dropping 2 mL of this solution directly into 10 mL of deionised water (pH = 7.8) at ambient temperature, to give a final aqueous polymer concentration of 1 mg mL^{-1} after organic solvent removal by evaporation. Both polymers generated stable nanoparticles and analysis was conducted by dynamic light scattering (DLS) to assess nanoparticle hydrodynamic diameters (D_z), zeta-potential (ζ) and polydispersity (PDI). Particles generated by the linear EBiB-initiated polymer were more polydisperse and considerably larger than the equivalent materials generated from the branched copolymer, as described previously (Table 2).[30]

Table 2. DLS analysis of nanoprecipitated particles from linear-dendritic polymer hybrids and *hyp*-polydendrons (measured at 25 °C).

Polymer	pH = 7.8[a]			pH = 4.0[a]		
	D_z (nm)	PDI	ζ (mV)	D_z (nm)	PDI	ζ (mV)
EBiB-*p*(HPMA$_{50}$), **14**	780	0.230	-33.7	-	-	-
G$_0$-*p*(HPMA$_{50}$), **15**	-	-	-	581	0.280	+52.0
G$_1$-*p*(HPMA$_{50}$), **16**	-	-	-	246	0.193	+40.3
G$_2$-*p*(HPMA$_{50}$), **17**				491	0.165	+43.7
EBiB-*p*(HPMA$_{50}$-*co*-EGDMA$_{0.95}$), **18**	151	0.077	-25.9	-	-	-
G$_0$-*p*(HPMA$_{50}$-*co*-EGDMA$_{0.9}$), **19**	157	0.269	-12.2	147	0.304	+54.9
G$_1$-*p*(HPMA$_{50}$-*co*-EGDMA$_{0.9}$), **20**	81	0.193	-32.2	102	0.271	+45.2
G$_2$-*p*(HPMA$_{50}$-*co*-EGDMA$_{0.9}$), **21**	132	0.097	-23.9	196	0.373	+60.9

[a] Initial pH of water used for nanoprecipitation

When the same nanoprecipitation conditions were used for the amine-functional linear-dendritic polymer hybrids **15**-**17** and *hyp*-polydendrons **19**-**21**, the linear materials were unable to form stable particles without macroscale precipitation, however, the *hyp*-polydendrons successfully generated nanoparticles for all generations of dendron end groups, Table 2. This difference is remarkable given the effect appears to be driven by branching and, potentially, the manner in which the polymers pack during the precipitation process. It is important to not ignore the difference in molecular weight between branched and linear materials, however, the individual *hyp*-polydendrons comprise different numbers of conjoined linear-dendritic hybrid chains, and a significant amount of linear material is also present within their molecular weight distributions. This has the impact of presenting the same overall number of primary chains and chain-ends in any physical mass of linear or branched polymer that is nanoprecipitated within this study. The fraction of branched materials within each sample is clearly capable of directing the behaviour of the overall distribution, possibly due to the presence of much larger nuclei being formed when the larger molecular weight *hyp*-polydendron structures respond to the changing solvent conditions than the smaller linear-dendritic hybrid equivalents (Figure 2). This may also explain the lower D_z values seen for **18** when compared to **14**, despite the much higher molecular weight and Đ values of **18** (Table 1).

The negative ζ value of the nanoprecipitates is consistent with previous reports of *p*(HPMA$_x$) and EBiB-*p*(HPMA$_x$-*co*-EGDMA$_y$) nanoprecipitation[22,30] and other hydrophobic nanoparticles in water; this has been explained in terms of adsorbed hydroxide ions for a range of material types including films of polystyrene and poly(hydroxyethyl methacrylate).[46-48] The presence of amine-functional dendrons of different generation at the chain-ends does not seem to greatly influence the measured ζ values at this pH and titrations of the individual dendron initiators **11**, **12** and **13** allowed an estimation of the pK_a values of the dendrons to be pK_a(G$_0$) ≈ 6.4, pK_a(G$_1$) ≈ 6.2 and pK_a(G$_2$) ≈ 6.2 suggesting a lack of protonation at this nanoprecipitation pH (Figure 3A). These pK_a values are similar to those of homopolymer polybases, such as poly(2-(diethylamino)ethyl) methacrylate, reported to have pK_a values between 6.9 and 7.4.[49,50]

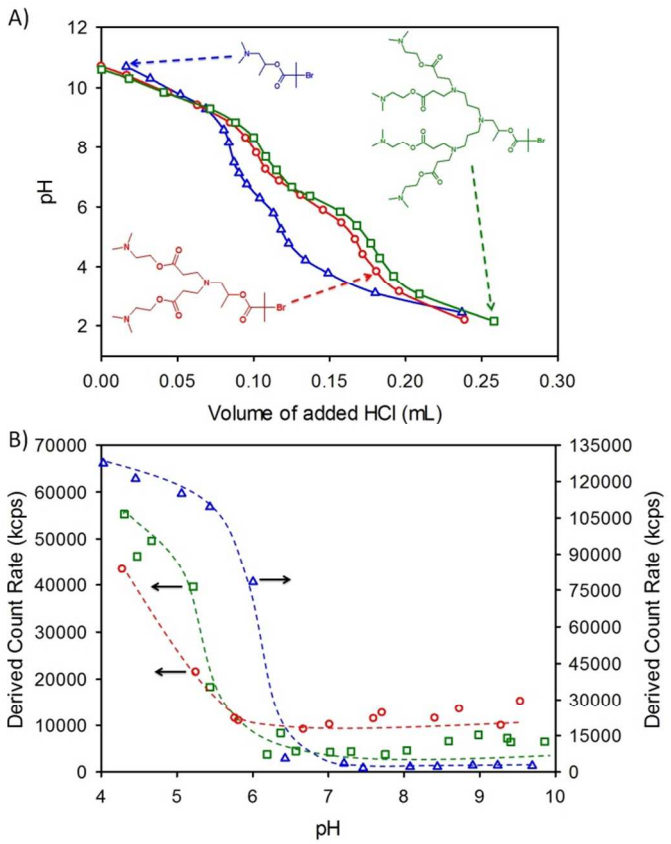

Figure 3. pH studies of A) G$_0$-G$_2$ dendron initiators leading to pK_a estimations (G$_0$-Br = blue open triangles, G$_1$-Br = red open circles and G$_2$-Br = green open squares), and B) Derived count rate (DLS) of nanoprecipitates of G$_x$-*p*(HPMA$_{50}$) linear-dendritic hybrids (G$_0$-*p*(HPMA$_{50}$) = blue open triangles, G$_1$-*p*(HPMA$_{50}$) = red open circles and G$_2$-*p*(HPMA$_{50}$) = green open squares) formed at pH = 4.0 and undergoing base titration. All DLS measurements were at 25 °C.

Impact of pH and aqueous salts on linear-dendritic hybrid and hyperbranched-polydendron nanoprecipitates.

The presence of amine-functional end groups offered the potential to compare the behaviour of linear-dendritic hybrids and *hyp*-polydendrons when nanoprecipitating into acidic water. All linear and hyperbranched polymers were insoluble at pH 4, and all but one polymer (G_2-*p*($HPMA_{50}$)) were insoluble at pH 2 (ESI Fig S30). We attribute this solubility trend to the density of amine groups on the G_2 dendron end group and the inability of the *p*($HPMA_{50}$) chains within the G_2-dendron containing *hyp*-polydendron to collapse independently. Identical conditions to those described above were used for each nanoprecipitation but the anti-solvent conditions employed aqueous HCl at pH 4.

As expected, the formation of charge-stabilised nanoparticles was not possible for **14** and **18** when nanoprecipitating into low pH water (Table 2) and both the linear and branched polymers initiated by EBiB underwent instant macroscale precipitation. All of the remaining linear-dendritic hybrids **15-17** and *hyp*-polydendrons **19-21** formed nanoparticles and the trend for *hyp*-polydendrons generating considerably lower D_z values (0.25-0.40 fold) than the linear-dendritic hybrids was again seen. Highly positive ζ values were also observed, even for materials bearing a single tertiary amine chain-end, as expected for protonated amine functionality and suggesting a significant number of dendron chain-ends present at the nanoparticle surfaces. The assembly of the polymers into large structures must also result in many dendron-carrying chain-ends being entrapped within the main bulk of the nanoprecipitate, as reported previously for *hyp*-polydendrons containing mixed PEG and hydrophobic dendron chain-ends.[22] In this case, the internalised dendrons would also be expected to be protonated after nanoprecipitation into acidic water and be somewhat hydrated. To study the response of the linear-dendritic hybrid and *hyp*-polydendron nanoprecipitates to changes in pH, the materials prepared in aqueous HCl were subjected to a titration through the slow addition of base (1M NaOH) with subsequent ζ measurement to establish isoelectric points (IEPs) for each nanoprecipitate. Interestingly, the nanoprecipitates formed from the linear-dendritic hybrids **15-17** were much more robust to the slow addition of NaOH during the titration than the corresponding *hyp*-polydendron nanoprecipitates which underwent considerable precipitation after the initial addition of base. Data for the *hyp*-polydendrons was therefore not reliable and stable ζ values were often difficult to obtain during the measurements. IEP measurements of the nanoprecipitates formed from **15-17** showed steadily decreasing ζ values with increasing addition of base and a relatively stable PDI value until pH values between 5.4-5.8. A corresponding decrease in the scattering intensity (derived count rate) from the samples during further titration was also observed (Figure 3B) corresponding to the onset of considerable precipitation. The observed decrease in derived count rate was considerably larger than would be expected after the maximum 1.3 fold dilution associated with the volumes of NaOH added during the titration to achieve high pH values.

Table 3. DLS analysis of nanoprecipitated particles from linear-dendritic polymer hybrids and *hyp*-polydendrons (measured at 25 °C).

Polymer	1M HCl[a] (Final pH = 3.6-4.1)			+ 1M NaOH (Final pH 11.5-11.9)			+ 1M HCl (Final pH 3.1-3.4)		
	D_z (nm)	PDI	ζ (mV)	D_z (nm)	PDI	ζ (mV)	D_z (nm)	PDI	ζ (mV)
G_0-*p*($HPMA_{50}$), **15**	581	0.280	+52.0	-	-	-	-	-	-
G_1-*p*($HPMA_{50}$), **16**	246	0.193	+40.3	158	0.197	-47.7	-	-	-
G_2-*p*($HPMA_{50}$), **17**	491	0.165	+43.7	162	0.279	-51.0	168	0.173	+32.3
G_0-*p*($HPMA_{50}$-*co*-$EGDMA_{0.9}$), **19**	147	0.304	+54.9	-	-	-	-	-	-
G_1-*p*($HPMA_{50}$-*co*-$EGDMA_{0.9}$), **20**	102	0.271	+45.2	96	0.143	-46.5	157	0.117	+30.5
G_2-*p*($HPMA_{50}$-*co*-$EGDMA_{0.9}$), **21**	196	0.373	+60.9	136	0.236	-47.8	163	0.130	+36.1

[a]Initial pH = 4.0

The determination of IEPs involves the slow addition of base, therefore, the rapid switching to basic and then acidic pH was also studied (Table 3). The rapid addition of base to the nanoparticles formed under acidic conditions from linear and branched polymers initiated by G_0 dendrons led to instant macroscale precipitation. Linear-dendritic hybrid and *hyp*-polydendron-derived nanoparticles containing G_1 or G_2 dendrons (2 or 4 amines per dendron respectively) were able to maintain stable nanoparticles without any indication of phase separation after fast base addition and attainment of a final solution pH ≈ 12. During the pH change to basic conditions, D_z values decreased for all samples with a concurrent switch from highly positive ζ to highly negative values. This decrease in D_z is consistent with deprotonation of the amine functional groups and the nanoparticles becoming overall more hydrophobic; dendrons present at the surface would be expected to collapse back onto the hydrophobic nanoparticle surface and dendrons within the nanoparticle interior, carrying protonated amines and bound water, would also be expected to become hydrophobic leading to a possible contraction of the overall structure as water is expelled (Figure 4).

Although this rationale may explain the relatively small changes (6-30%) seen within the *hyp*-polydendron derived nanoparticles, with the largest initial change observed for the G_2-derived material **21**, the nanoparticles from the linear-dendritic hybrids showed a larger change in D_z (36-67%), again with the largest change being observed for the G_2-derived linear polymer **17**. This may suggest a more complicated rearrangement of the nanoparticle structures generated from linear–dendritic hybrids as each small linear polymer has a greater degree of freedom during particle formation than their branched analogues.

Further rapid addition of 1M HCl to these samples to change back to an acidic environment, led to precipitation of the nanoparticles formed from G_1-*p*(HPMA$_{50}$) **16**. The nanoparticles derived from the linear-dendritic hybrid **17**, with a G_2 dendron end group, and both *hyp*-polydendron nanoprecipitates containing G_1 and G_2 dendron end groups (**20** and **21**) maintained colloidal stability whilst switching their zeta-potential back to highly positive values and undergoing a slight increase in D_z; as previously, no precipitation was observed during this rapid change in pH for these materials. The small increase in size across these materials may be due to the lack of penetration of the acid into the hydrophobic core structures, formed during base addition, and protonation only occurring at the surface (and near surface) dendrons leading to very limited swelling (Figure 4). The only anomaly was seen with the G_1-*p*(HPMA$_{50}$-*co*-EGDMA$_{0.9}$) *hyp*-polydendron that resulted in a larger final D_z than immediate values determined after nanoprecipitation into acid. An explanation for this is not immediately obvious; however, all final materials exhibited very similar diameters (157-168 nm) in acid after the two pH switches.

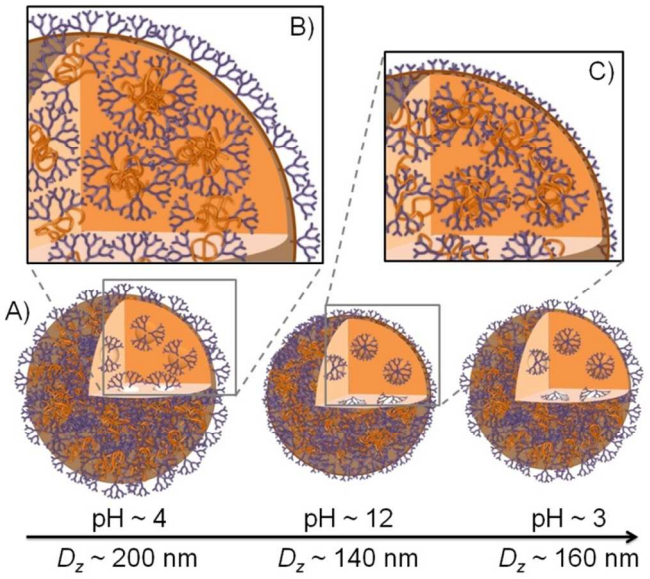

Figure 4. Diagrammatic representation of amine-functional hyperbranched-polydendron nanoprecipitates formed at pH=4 and change in solvation of the core and surface dendrons: A) deprotonation and collapse of amine-functional dendrons on addition of base, with subsequent protonation of surface functional groups on addition of acid, B) representation of protonated and hydrated exterior and interior dendrons with collapsed vinyl polymer chains within the hyperbranched-polydendron structure, C) deprotonated and collapsed structure of dendrons and vinyl polymer chains

An additional experiment where G_2-*p*(HPMA$_{50}$-*co*-EGDMA$_{0.9}$) and G_2-*p*(HPMA$_{50}$) were individually nanoprecipitated directly into aqueous NaOH (pH = 12) was conducted to determine the nature of the resulting nanoprecipitates within this medium. Interestingly, both materials generated nanoprecipitates with very similar size and zeta potentials to those having been initially formed in acid and later treated with base (G_2-*p*(HPMA$_{50}$): D_z = 152 nm, PDI = 0.081, ζ = -46.0 mV; G_2-*p*(HPMA$_{50}$-*co*-EGDMA$_{0.9}$): D_z = 127 nm, PDI = 0.135, ζ = -43.1 mV). The same trend of smaller particles being formed from *hyp*-polydendrons compared to those from their linear analogues was seen once again

The stability of nanoparticles to added salt is an important property for many possible applications. As shown in Table 2, the linear-dendritic hybrid polymers were unable to generate nanoprecipitates through direct precipitation into water at pH 7.8, however, the equivalent *hyp*-polydendrons generated stable nanoparticles. We have previously shown that salt stability is not present for nanoprecipitates generated by EBiB-*p*(HPMA$_x$-*co*-EGDMA$_y$) polymers produced at near neutral pH,[30] but the modification of the end-groups with amine functionality provides the potential to modify this behaviour.

The three nanoprecipitates prepared at pH 7.8 from *hyp*-polydendrons **19**, **20** and **21** were treated with 0.14 M aqueous NaCl by adding 1 mL of this salt solution to a 10 mL volume of nanoparticles at a concentration of 1 mg/mL. All *hyp*-polydendron nanoprecipitates were stable to added salt (SI Fig S31) with little or no substantial change in D_z values being observed over 24 hours (SI Table S3). It is important to note that no studies have indicated any degradation of the polymers or dendrons over the timescales of these studies.

Mechanistic interpretation of the observed behaviour of amine functional hyperbranched polydendron nanoprecipitates.

According to DLVO theory,[51,52] the balance of electrostatic repulsion and van der Waals attraction will determine nanoparticle stability and the addition of salt is known to strongly decrease the Debye length through screening of charge and decreasing the distance over which the effects of electrostatics persist. The low generation of the dendrons present throughout this study would not be expected to provide steric stabilisation against the approach of two nanoparticles and no barrier to the attractive van der Waals attraction would therefore be present. As such, the electrostatic interactions are believed to dominate the behaviour of the materials being studied.

As stated earlier, the adsorption of hydroxide ions to hydrophobic surfaces is a phenomenon that has been described for many material types, often leading to the observation of negative ζ values for a range of materials including emulsion droplets. This assertion has been modelled using molecular dynamics simulations[47] of ions held between two hydrophobic plates, suggesting that the physisorption of hydroxide ions is thermodynamically favourable and driven by the preferential orientation of two layers of water molecules at the hydrophobic surface after hydroxide adsorption. Hydroxide ions from water auto-dissociation are also believed to be the source of negative ζ values measured in pure water; although the bulk hydroxide ion concentration is low in this case, the adsorption of hydroxide ions onto various surfaces (including non-ionic substrates) is expected to lead to appreciable localised concentrations at the water/solid, water/oil or water/gas interface.[47]

Here, the materials studied vary from out previous reports of $p(HPMA_x)$ and EBiB-$p(HPMA_x$-*co*-$EGDMA_y)$ only in the presence of varying numbers of tertiary amines at the dendron functional end groups. Our slow titration studies, the variation of ζ values with nanoprecipitation into acid and the rapid changes of pH, strongly indicate a substantial number of dendron end groups at the surface of the nanoprecipitates. Although electrostatics provide the dominant contribution to nanoparticle stabilisation, the tolerance to salt and the ability to rapidly switch pH through the IEP without aggregation, for some materials, is most certainly derived from the presence of the tertiary amine-functional end groups. These end groups will clearly modify the surface chemistry of the nanoparticles over those derived purely from EBiB-$p(HPMA_x$-*co*-$EGDMA_y)$, and the dendron generation contributes a varying tertiary amine surface density derived from both the terminal and branch points of each dendron (G_0 = 1 NR_3; G_1 = 3 NR_3; G_2 = 7 NR_3 groups).

Computational estimations of octanol-water partition coefficients, logP, (miLogP2.2 derived using the molinspiration property engine; see ESI Fig S32) have been conducted for the G_0-G_2 dendron fragments to assess how the hydrophobicity of the presented nanoparticle surface may vary across the nanoprecipitates. Group contribution calculations for logP depend on the fragment chosen for analysis and are therefore only indicative; however, the chosen G_0-G_2 fragments generated logP values of 1.690, 1.399 and 1.709 respectively. This appears to suggest each dendron is significantly hydrophobic and that the G_1 dendron presents a slightly less hydrophobic end-group than either the G_0 or G_2 dendron end groups. Variation of the chosen fragment to include the first HPMA monomer unit (ESI Fig S33), for comparative purposes, resulted in higher values, but the trend of hydrophobicity and the order $G_2 \approx G_0 > G_1$ was preserved.

The ability to rapidly switch pH within these materials seems to be restricted to G_1 and G_2-functional materials, which may indicate that a relatively high density of amine groups is important. As the medium is switched to high pH, the amines will become hydrophobic and the adsorption of hydroxide ions will be driven by the surface chemistry, which in turn will be controlled by the amine density within the dendrons. Quickly achieving a high negative ζ during this process is critical to stabilise the nanoparticles before aggregation. The rate of adsorption would be expected to be a function of surface hydrophobicity, however, the logP estimations suggest that this is not necessarily the main factor controlling the adsorption as G_0 dendron fragments appear to have a higher logP than G_1 dendron fragments. As such, the amine density and the potential for hydrogen bonding with hydroxide ions and water may act to enhance the attainment of negative ζ values during the rapid pH switch to basic conditions. Switching back to acidic pH requires the rapid attainment of a sufficiently positive ζ to overcome van der Waals attractive forces and, again, a relatively high density of tertiary amines per dendron would be expected to become quickly protonated and generate a significant charge.

An estimation of the impact of dendron generation on the number of amines at the nanoprecipitate surface can be readily generated when considering a series of nominal nanoprecipitates with a diameter of 100 nm and dendron chain-ends of varying generation. If the chain-ends are considered as spheres and a simple close packing is assumed (cubic close packing and hexagonal close packing have a density of 0.74), the diameter of each sphere will dictate a circular surface area occupied by each chain-end. A group contribution model (molinspiration property engine) was used to estimate the molecular volume of each of the dendrons by utilising the fragments including the first HPMA monomer residue (Figure 5A), previously used to calculate logP values (ESI Fig S33).

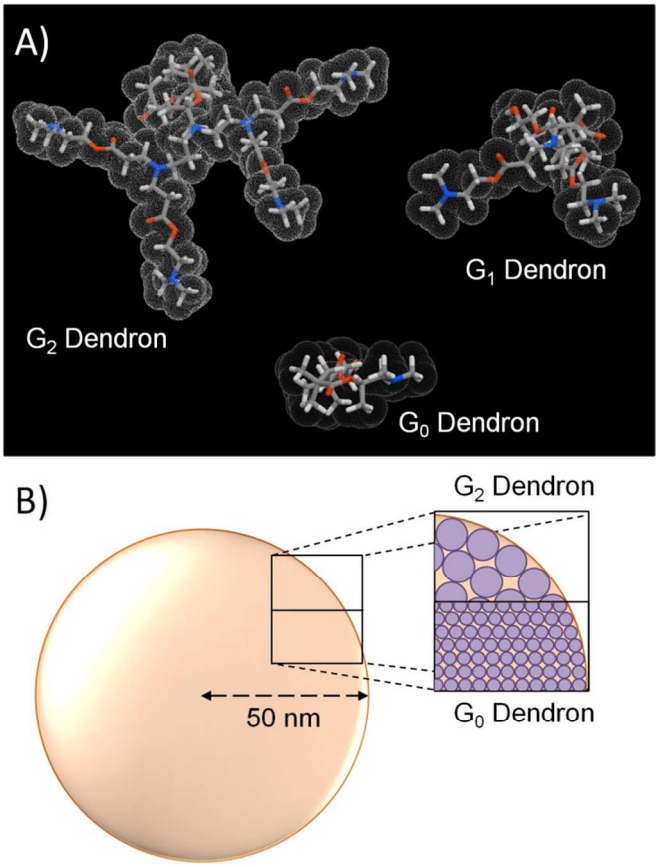

Figure 5. Consideration of amine density at the nanoprecipitate surface. A) Molinspiration property engine determination of the confirmation and volume of G_0-G_2 dendron polymer chain-ends, and B) schematic variation of number of dendrons packing at the nanoparticle surface.

The calculated molecular volumes (G_2-dendron fragment = 996 $Å^3$; G_1-dendron fragment = 587 $Å^3$; G_0-dendron fragment = 338 $Å^3$) were used to generate radii for each hypothetical circular surface area. Simple division of the 100 nm diameter nanoprecipitate surface area (31420 nm^2) by the surface area occupied by each dendron estimated that, in a close packed model (density of 0.74), the number of chain-ends at each surface would vary from approximately 20000 for the G_2-dendron to 28000 for the G_1-dendron and 40000 for the G_0-dendron (Figure 5B). When multiplying by the number of

tertiary amines per dendron (see above), however, the number of amines occupying the surface of each hypothetical nanoprecipitate varies from approximately 182000 for the G_2-dendron to 111000 for the G_1-dendron and 40000 for the G_0-dendron. This would, in principle, be seen in both linear-dendritic hybrid and *hyp*-polydendron nanoprecipitates and it is noticeable that only the G_2-functional linear-dendritic hybrid was able to tolerate the switching from acid to base and back to acid again, whilst both the G_1 and G_2-functional *hyp*-polydendrons could achieve this. In addition, the topological polar surface areas (TPSA), calculated using the SMILES code (simplified molecular-input line-entry system) of each chain-end fragment were estimated using a 2D model, first proposed by Ertl *et al*,[53] that considers the contribution of polar atoms (N, C and H) within the fragment structure with validation against 3D molecular polar surface area calculations; TPSA values of approximately 200 $Å^2$ for the G_2-dendron, 135 $Å^2$ for the G_1-dendron and 76 $Å^2$ for the G_0-dendron were calculated. These, again, suggest a highly variable contribution to the surface chemistry of the nanoprecipitates resulting from each material studied.

The question of why the IEP titrations were difficult to perform with the *hyp*-polydendron nanoprecipitates and why branching would impact the other observed behaviour of otherwise chemically identical materials remains and this may be related to the mechanism of nanoparticle generation during nanoprecipitation at low pH and also the different amine densities at the surface of the nanoparticle. The formation of large nuclei from the most branched structures appears to direct nanoprecipitation of *hyp*-polydendrons. This is a highly cooperative process as the large numbers of conjoined chains (weight average *hyp*-polydendron structures contain between >17-65 linear chains) will be unable to relax independently and the chemical differences of the protonated chain-ends and the desolvated hydrophobic vinyl polymer chains will generate phase separated, possibly core-shell, structures. As such, the formation of nanoprecipitates from *hyp*-polydendrons may be more akin to the packing of spheres of mixed diameters rather than the sole adsorption of unimers to a growing nanoparticle surface. Within the nanoprecipitation of the linear-dendritic hybrids, this process is conducted on a chain-by-chain basis and without the cooperative behaviour of the large branched structures. If the packing of species within the *hyp*-polydendron nanoprecipitate leads to a larger density of surface dendrons, these materials would be expected to achieve colloidal stability through charge repulsion more rapidly during the growth phase of the nanoprecipitation, leading to lower D_z values as observed. A high density of tertiary amines on the surface of the *hyp*-polydendron nanoprecipitates may, however, impair overall protonation, leading to a lower total number of positively charged tertiary amines, especially as branching structures will prevent charge separation. This has previously been reported with respect to the notable suppression of a rheological increase (the so-called polyelectrolyte effect) during the deprotonation of branched vinyl polyacids.[54] The slow addition of base during the IEP titrations would therefore be expected to readily generate hydrophobic areas on the surface of the *hyp*-polydendron nanoprecipitates, leading to aggregation and precipitation. Subtle changes in polymer end-groups have been shown previously to impact on the behaviour of polymers in aqueous solutions[55] and the case studied here does represent a relatively extreme case of material behavioural control from both chain-end chemistry and polymer architecture.

Salt tolerance may also be driven by an enhanced adsorption of hydroxide ions onto amine functional nanoparticles which modifies the screening of charge on addition of electrolyte.

Conclusions

The presented data demonstrates a new approach to the rapid formation of low generation amine-functional dendrons, the modification of the dendrons into ATRP initiators and the controlled formation of linear-dendritic hybrids and *hyp*-polydendrons. The nanoprecipitates derived from the materials are unique and display behaviour that appears to benefit from both the presence and generation of the dendron end groups and the branching of the methacrylate polymer chains. A model to explain the varying behaviour of linear-dendritic polymer analogues of *hyp*-polydendrons is presented that assumes a different arrangement of dendrons and vinyl polymer segments within the nanoprecipitates, directed predominantly by the branched polymer architecture and the chemical dissimilarity of the charged chain-ends and the uncharged and collapsed polymer chains. These differences appear to modify the ability of the nanoparticle surfaces to protonate and deprotonate, presumably leading to rapid hydroxide adsorption in the deprotonated state. Applications of these materials are being studied and further investigations are needed to fully quantify the proposed mechanistic interpretation of the observed behaviour, but the flexibility and ease of synthesis and nanoparticle formation does suggest that these materials have the potential to offer platform benefits.

Acknowledgement

The authors acknowledge the University of Liverpool and EPSRC for funding (Grant number EP/I038721/1) and Doctoral Training Awards for HER, FYH and SA (EP/H000925 – Programme Grant). The Centre for Materials Discovery is also thanked for access to electron microscopy facilities.

Notes and references

[a] Department of Chemistry, University of Liverpool, Crown Street, Liverpool L69 7ZD, United Kingdom. E-mail: srannard@liv.ac.uk
[b] Department of Molecular and Clinical Pharmacology, University of Liverpool, Block H, 70 Pembroke Place, Liverpool L69 3GF, UK

Electronic Supplementary Information (ESI) available: Materials, experimental procedures and characterization data with assignments. See DOI: 10.1039/c000000x/

1. E. Buhleier, W. Wehner and F. Vögtle, *Synthesis*, 1978, **2**, 155.
2. D. A. Tomalia, H. Baker, J. Dewald, M. Hall, G. Kallos, S. Martin, J. Roeck, J. Ryder and P. Smith, *Polym. J.*, 1985, **17**, 117.
3. G. R. Newkome, Z. Yao, G. R. Baker and V. K. Gupta, *J. Org. Chem.*, 1985, **50**, 2003.
4. J. Satija, V. V. R. Sai, and S. Mukherji, *J. Mater. Chem.*, 2011, **21**, 14367.
5. X. Zhang, Y. Zeng, T. Yu, J. Chen, G. Yang and Y. Li, *J. Phys. Chem. Lett.*, 2014, **5**, 2340.
6. P. Kesharwani, K. Jain and N. K. Jain, *Prog. Polym. Sci.*, 2014, **39**, 268.
7. B. Huang, S. Tang, A. Desai, K-H Lee, P. R. Leroueil and J. R. Baker, *Polymer*, 2011, **52**, 5975.
8. J. Wang and T. Xu, *Polym. Advan. Technol.*, 2011, **22**, 763.
9. R. S. Navath, A. R. Menjoge, B. Wang, R. Romero, S. Kannan and R. M. Kannan, *Biomacromolecules*, 2010, **11**, 1544.
10. C. J. Hawker and J. M. J. Fréchet, *Macromolecules*, 1990, **23**, 4726.
11. J. Tolosa, C. Romero-Nieto, E. Diez-Barra, P. Sanchez-Verdu and J. Rodriguez-Lopez, *J. Org. Chem.*, 2007, **72**, 3847.
12. H. Willcock, A. I. Cooper, D. J. Adams and S. P. Rannard, *Chem. Commun.*, 2009, 3095.
13. J. M. J. Fréchet, C. J. Hawker and K. L. Wooley, *J. Macromol. Sci. A*, 1994, **31**, 1627.
14. J. M. J. Fréchet, C. J. Hawker, I. Gitsov and J. W. Leon, *J. Macromol. Sci. A*, 1996, **33**, 1399.
15. a) G. R. Newkome and C. D. Shreiner, *Polymer*, 2008, **49**, 1; b) M. V. Walter and M. Malkoch, *Chem. Soc. Rev.*, 2012, **41**, 4593.
16. X. Sun, J-P. Lindner, B. Bruchmann and A. D. Schluter, *Macromolecules*, 2014, **47**, 7337.
17. A. D. Schluter, A. Halperin, M. Kroger, D. Vlassopoulos, G. Wegner and B. Zhang, *ACS Macro Lett.*, 2014, **3**, 991.
18. C. M. B. Santini, T. A. Hatton, and P. T. Hammond, *Langmuir*, 2006, **22**, 7487.
19. S. E. R. Auty, O. C. J. Andrén, F. Y. Hern, M. Malkoch and S. P. Rannard, *Polym. Chem.*, 2015, **6**, 573.
20. O. C. J. Andrén, M. V. Walter, T. Yang, A. Hult and M. Malkoch, *Macromolecules*, 2013, **46**, 3726.
21. F. L. Hatton, P. Chambon, T. O. McDonald, A. Owen and S. P. Rannard, *Chem. Sci.*, 2014, **5**, 1844.
22. F. L. Hatton, L. M. Tatham, L. R. Tidbury, P. Chambon, T. He, A. Owen and S. P. Rannard, *Chem. Sci.*, 2015, **6**, 326.
23. N. O'Brien, A. McKee, D. C. Sherrington, A. T. Slark and A. Titterton, *Polymer*, 2000, **41**, 6027.
24. S. Graham, S. P. Rannard, P. A. G. Cormack and David C. Sherrington, *J. Mater. Chem.*, 2007, **17**, 545.
25. J. M. J. Fréchet, M. Henmi, I. Gitsov, S. Aoshima, M. R. Leduc and R. B. Grubbs, *Science*, 1995, **269**, 1080.
26. C. Li, H. Liu, D. Tang and Y. Zhao, *Polym. Chem.*, 2015, **6**, 1474.
27. W. J. Feast, S. P. Rannard and A. Stoddart, *Macromolecules*, 2003, **36**, 9704.
28. A. Stoddart, W. J. Feast and S. P. Rannard, *Soft Matter*, 2012, **8**, 1096.
29. S. P. Rannard and N. J. Davis, *Org. Lett.*, 1999, **1**, 933.
30. R. A. Slater, T. O. McDonald, D. J. Adams, E. R. Draper, J. V. M. Weaver and S. P. Rannard, *Soft Matter*, 2012, **8**, 9816.
31. I. Bannister, N. C. Billingham, S. P. Armes, S. P. Rannard and P. Findlay, *Macromolecules*, 2006, **39**, 7483.
32. E. Blasco, M. Piñol and L. Oriol, *Macromol. Rapid Commun.*, 2014, **35**, 1090.
33. C-M. Dong and G. Liu, *Polym. Chem.*, 2013, **4**, 46.
34. a) Y. Bi , C. Yan , L. Shao , Y. Wang , Y. Ma and G. Tang , *J. Polym. Sci. Polym. Chem.*, 2013, **51**, 3240; b) Y. Hed, Y. Zhang, O. C. J. Andrén, X. Zeng, A. M. Nyström, and M. Malkoch, *J. Polym. Sci. Polym. Chem.*, 2013, **51**, 3992.
35. L. Zhu , G. Zhu , M. Li , E. Wang , R. Zhu and X. Qi, *Eur. Polym. J.*, 2002, **38**, 2503.
36. H.-il Lee, J. A. Lee, Z. Poon and P. T. Hammond, *Chem. Commun.*, 2008, 3726.
37. J. C. M. van Hest, M. W. P. L. Baars, C. Elissen-Román, M. H. P. van Genderen and E. W. Meijer, *Macromolecules*, 1995, **28**, 6689.
38. S. Khoee and K. Hemati, *Polymer*, 2013, *54*, 5574.
39. L. Chen, T. Chen, W. Fang, Y. Wen, S. Lin, J. Lin and C. Cai, *Biomacromolecules*, 2013, **14**, 4320.
40. E. R. Gillies, T. B. Jonsson and J. M. J. Fréchet, *J. Am. Chem. Soc.*, 2004, **126**, 11936.
41. Y. Oikawa, S. Lee, D. H. Kim, D. H. Kang, B.-S. Kim, K. Saito, S. Sasaki, Y. Oishi and Y. Shibasaki, *Biomacromolecules*, 2013, **14**, 2171.
42. Z. Ge, S. Luo and S. Liu, *J. Polym. Sci. Polym. Chem.*, 2006, **44**, 1357.
43. S. Schubert, J. T. Delaney and U. S. Schubert, *Soft Matter*, 2011, 7, 1581.
44. C. Zhang, V. J. Pansare, R. K. Prud'homme and R. D. Priestley, *Soft Matter*, 2012, **8**, 86.
45. C. E. Mora-Huertas, H. Fessi and A. Elaissari, *Int. J. Pharm.*, 2010, **385**, 113.
46. S. Inphonlek, N. Pimpha and P. Sunintaboon, *Colloid. Surface. B*, 2010, **77**, 219.
47. R. Zangi and J. B. F. N. Engberts, *J. Am. Chem. Soc.*, 2005, **127**, 2272.
48. R. A. van Wagenen, D. L. Coleman, R. N. King, P. Triolo, L. Brostrom, L. M. Smith, D. E. Gregonis abd J. D. J. Andrade, *Colloid Interface Sci.*, 1981, **84**, 155.
49. A. J. Morse, S. P. Armes, P. Mills, and R. Swart, *Langmuir*, 2013, **29**, 15209.
50. J. Hu, G. Zhang, Z. Ge and S. Liu, *Prog. Polym. Sci.*, 2014, **39**, 1096.
51. B. V. Derjaguin and L. D. Landau, *Acta Physicochim.URS.*, 1941, **14**, 633.
52. E. J. W. Verwey and , J. T. G. Overbreek, "Theory of the Stability of Lyophobic Colloids, the Interaction of Sol Particles Having an Electrical Double Layer"; Elsevier: Amsterdam, The Netherlands, 1948.
53. P. Ertl, B. Rohde, P. Selzer, *J. Med. Chem.*, 2000, **43**, 3714.
54. S. Graham, P. A. G. Cormack and D. C. Sherrington, *Macromolecules*, 2005, **38**, 86.
55. S. Jana, S. P. Rannard and A. I. Cooper, *Chem. Commun.*, 2007, 2962.

